Dyes and Pigments 80 (2009) 254–258

Contents lists available at ScienceDirect

Dyes and Pigments

journal homepage: www.elsevier.com/locate/dyepig

The biomimetic synthesis of zinc phosphate nanoparticles

Shunpu Yan [a], Wen He [a,b,*], Caiyun Sun [c], Xudong Zhang [a], Hongshi Zhao [a], Zhengmao Li [a], Weijia Zhou [a], Xiuying Tian [a], Xianan Sun [a], Xiuxiu Han [a]

[a] Department of Materials Science and Engineering, Shandong Institute of Light Industry, Jinan 250353, PR China
[b] Biomaterials Research Center, South China University of Technology, Guangzhou 510640, PR China
[c] State Key Lab of Microbial Technology, Shandong University, Jinan 250100, PR China

ARTICLE INFO

Article history:
Received 15 April 2008
Received in revised form 3 June 2008
Accepted 12 June 2008
Available online 22 July 2008

Keywords:
Zinc phosphate
Chemical precipitation
Nanoparticle
Yeast cell
Biomimetic synthesis
Anticorrosion

ABSTRACT

A generic approach, based on the basic principles of biomineralization, has been applied to the synthesis of zinc phosphate nanoparticles by chemical precipitation using yeast cells. UV, XRD, FTIR, and SEM were employed to characterize the product. The single-stage synthesis is cost-effective, easy to control and is performed at low temperature and normal pressure. The mechanism of the formation of $Zn_3(PO_4)_2$ nanoparticles was studied.

1. Introduction

The creation of nano-materials for advanced structures has led to a growing interest in the area of biomineralization. Numerous microorganisms are capable of synthesizing inorganic-based structures [1,2]. In biological systems, a large variety of organisms form organic/inorganic composites with ordered structures by the use of biopolymers such as protein and microbe cells, which have defined monomer sequences and controlled three-dimensional structures [3–5]. The process of biomineralization and the assembly of nanostructured inorganic components into hierarchical structures have led to the development of a variety of approaches that mimic the recognition and nucleation capabilities that occur in biomolecular inorganic synthesis [6–10]. Several studies have demonstrated that biomolecules identified from biological organisms can be used as enzymes or templates for material synthesis in vitro to control the nucleation and growth of the inorganic structure [11–13].

In the past decade, the crystallization of inorganic compounds on solid organic templates has attracted a great deal of attention. For example, diatoms used amorphous silica as structural materials [14], bacteria synthesized magnetite (Fe_3O_4) particles and form silver nanoparticles, and collagen, cholesterol, elastin and chitin showed significant effects on the control of $CaCO_3$ crystallization [15–18].

Inspiration for the synthesis of zinc phosphate nanoparticles described herein comes from earlier reports on the biosynthesis of silver [14,19], calcium carbonate [15–18] and other nanocrystals by bacterial cells [14] and organic macromolecules. Zinc phosphate, as a new type of non-toxic, ecological anticorrosive pigment with excellent properties, has been employed in the coating industry widely. However, owing to its low activity resulting from reunion and the dimension of big particles, it cannot replace traditional toxic anticorrosive pigments completely [20]. As a consequence, the preparation of zinc phosphate powders with mono-dispersion and narrow-size distribution is urgent so as to develop a new generation of zinc phosphate pigments of high performance. Many techniques such as hydrothermal, sol–gel technique and solid-state reactions have been employed to prepare zinc phosphate. It is evident that every method has its own shortcomings. Hydrothermal method needs high temperature and pressure [21]. It is expensive to synthesize zinc phosphate by sol–gel technique. To our best knowledge, no particles less than 1 μm were prepared by solid-state reactions [22]. Compared to the methods above, the chemical precipitation method in the presence of yeasts provides flexibility of operation and simplicity.

The object of this paper is to prepare nanoscale, easily dispersed, anticorrosive zinc phosphate using yeast templates; the reaction of zinc sulfate heptahydrate and trisodium phosphate was employed

* Corresponding author. Department of Materials Science and Engineering, Shandong Institute of Light Industry, Jinan 250353, PR China. Tel./fax: +86 531 88522792.
E-mail address: hewen19602008@126.com (W. He).

0143-7208/$ – see front matter © 2008 Elsevier Ltd. All rights reserved.
doi:10.1016/j.dyepig.2008.06.010

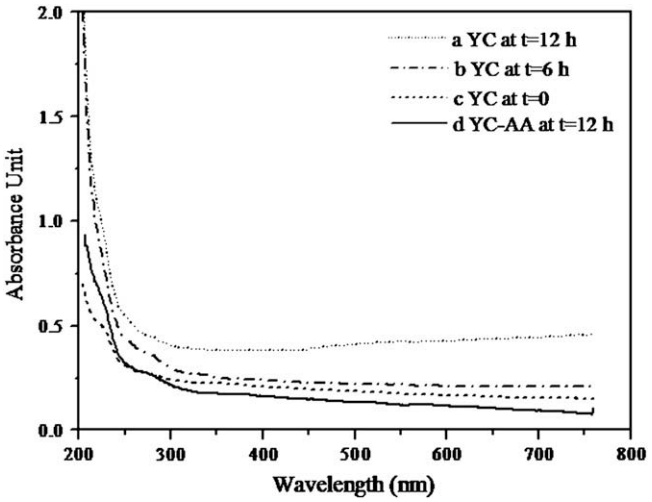

Fig. 1. UV spectra of yeast cells mixed with 0.1 M of $ZnSO_4$.

as a control. The fabrication of $Zn_3(PO_4)_2$ nanoparticles is studied, and the effects of yeasts on the formation and reunion of media are also discussed.

2. Experimental

2.1. Materials and methods

The starting materials used in this study include zinc sulfate heptahydrate ($ZnSO_4 \cdot 7H_2O$, 99.0%, Tianjin Baishi Chemical and Industry Ltd), trisodium phosphate dodecahydrate ($Na_3PO_4 \cdot 12H_2O$, 99.0%, Tianjin Baishi Chemical and Industry Ltd) and single-celled yeast microbes (Angel Yeast Co., Ltd). All chemical reagents are of analytical grade. Deionized water was used throughout the experiment.

2.1.1. Preparation of $Zn_2(PO_4)_3$/YCs

Firstly, 2.00 g of dry yeasts were cultivated in glucose aqueous solution (2 wt.%, 50 ml) at a temperature of 36 °C for 30 min. Then the as-prepared mixture was poured into an aqueous solution of zinc sulfate (0.1 M, 150 ml) to obtain the yeast/zinc mixture which was stirred for 24 h at room temperature. After the mixture was stirred for 24 h, Na_3PO_4 aqueous solution (0.1 M, 100 ml) was gradually added drop by drop under stirring condition, then continue stirring the mixture for 2 h and let it age for 48 h. An aqueous solution of NaOH (0.05 M) was employed to adjust the pH value of the reaction solution to 8–10 which was the range of the presence of zinc phosphate precipitation. Finally, the deposition was collected from the mixture by centrifugation at a rotation speed of 4500 rpm. The deposition was washed by distilled water until the conductivity of the filtrate was less than 2 ms/m and washed by ethanol once. The resultant powders were dried at 80 °C for 24 h.

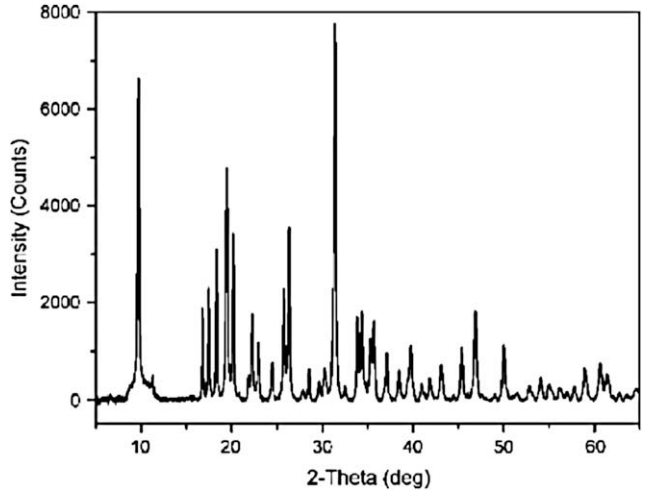

Fig. 2. XRD pattern of the as-prepared $Zn_3(PO_4)_2$ particles.

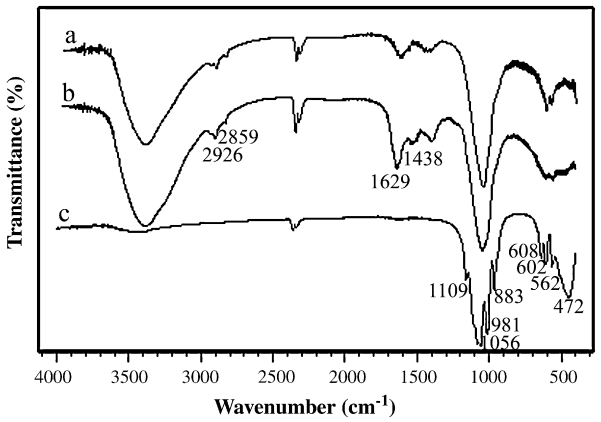

Fig. 3. FTIR spectra of $Zn_3(PO_4)_2$ without (a) and with (b) yeast cells. $Zn_3(PO_4)_2$ with yeast cells was calcined at (c) 750 °C for 2 h.

2.1.2. Preparation of yeast cells–acrylic acid (YC–AA)

An aqueous solution of 3 wt.% acrylic acid (AA) was gradually added into the as-prepared mixture of yeasts until the conductivity of the mixture got to the minimum. Then, the mixture was treated in the process of preparing $Zn_2(PO_4)_3$/YCs.

2.2. Characterization

Ultraviolet–visible spectrum (UV757, Shanghai) was used to observe the conjunction between zinc ions and functional groups. X-ray diffraction (XRD) patterns of samples were obtained on a Panalytical X'Pert PRO (PANalytical, Netherlands) using Cu Ka ($\lambda = 0.15418$ nm) radiation. The crystallite size of $Zn_3(PO_4)_2$ particles was estimated from the FWHM of XRD peaks according to Scherrer equation. Fourier transform infrared (FTIR) spectra were collected on a Nicolet Nexus spectrometer by using a KBr wafer technique in order to study the composition of the samples. The morphologies of the products were observed by scanning electron microscopy (S-4800, Hitachi).

3. Results and discussion

3.1. Ultraviolet–visible spectroscopy analysis

The ultraviolet–visible absorption profile for zinc sulfate solution mixed with yeasts and YC–AA is shown in Fig. 1. When the YCs and YC–AA were incubated in an aqueous solution of 0.1 mM zinc sulfate for 12–24 h at room temperature, series of changes were measured by ultraviolet–visible spectroscopy. Though no distinct surface plasmon characteristic absorption band at 200–800 nm was observed in our zinc sulfate solution incubated with the yeasts in the case of no developer, we found that the intensity became strong and curves a and b shift to red side along with the time. It may be imputed to the increase of homogeneous ligands around zinc ions. Unlike YC, the intensity of the UV spectrum of the YC–AA solution

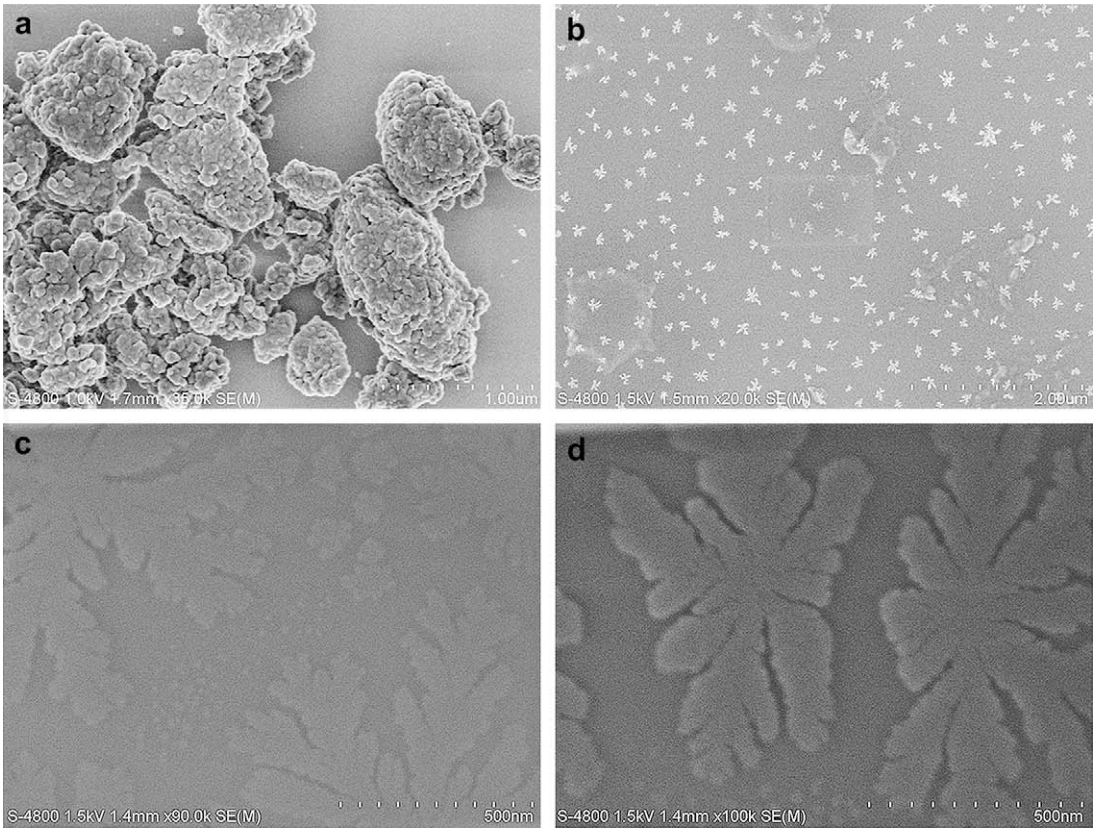

Fig. 4. SEM micrographs of $Zn_3(PO_4)_2$ without yeast cells (a) and with yeast cells (b). (c) and (d) Magnification of (b).

showed no distinct modification comparing with YC at $t = 0$. The main biochemical difference between the YC and YC–AA is the overall charges of the vesicle—esterification occurred and hydroxyl groups were protected when acrylic acid was added [16]. It demonstrates that hydroxyl groups on the cells play a key role in the synthesis of the material. Based on the above results, yeasts are capable of conjugation with zinc ions from an aqueous solution and the pivotal factor is the hydroxyl groups on biomacromolecules.

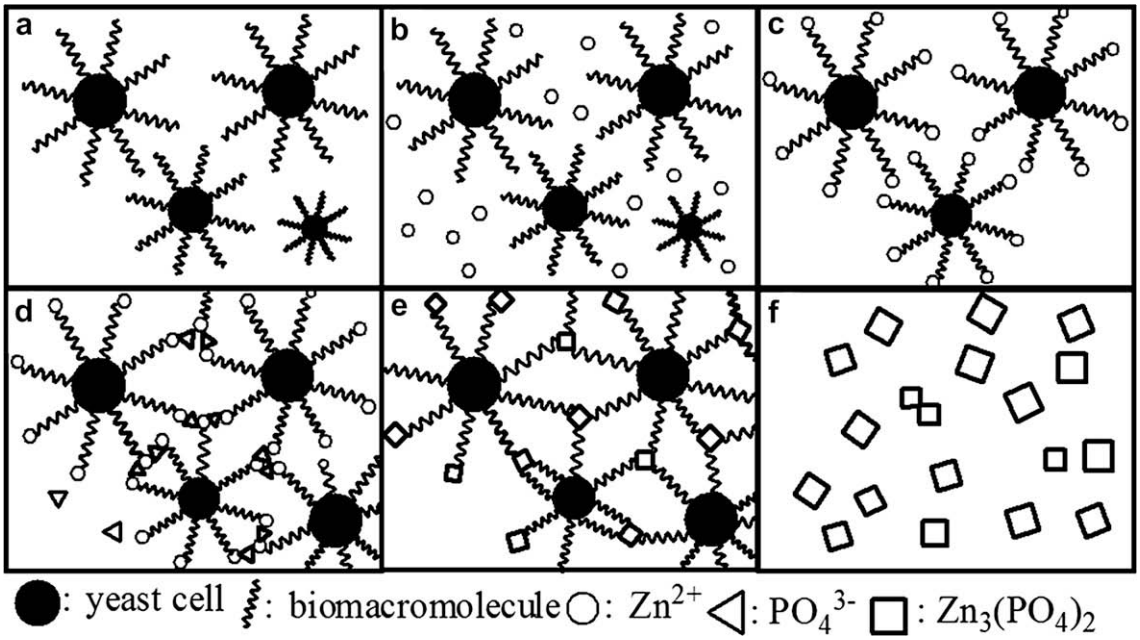

Fig. 5. Schematic diagrams of the interaction processes. When the as-incubated yeast cells (a) poured into an aqueous solution of 0.1 mM zinc sulfate (b), zinc ions first bond with the biomacromolecules on the pericellular membranes (c). The coming of phosphate radicals generates grains of crystallization (d) on the site of YC–Zn^{2+}. Crystals grew bigger and loose envelopes might be coated on the cells [29,30] (e). Scour off the templates, homogeneous particles can be obtained (f).

Table 1
Comparison of acid, alkali and salt resistance between as-prepared zinc phosphate, and commercial zinc phosphate, zinc chrome yellow, red lead

Solution	As-prepared $Zn_3(PO_4)_2$ (h)	Commercial $Zn_3(PO_4)_2$ (h)	Zinc chrome yellow (h)	Red lead (h)
3 wt.% NaOH	>50	>43	>45	>45
3 wt.% NaCl	>186	>175	>191	>149
3 wt.% H_2SO_4	>49	>40	>45	>45

3.2. XRD analysis

The XRD pattern of the as-prepared material is shown in Fig. 2. All peaks in the figure are indexed to the lattice of $Zn_3(PO_4)_2 \cdot 4H_2O$. The narrow and high peaks reveal that the as-prepared $Zn_3(PO_4)_2$ has a very small size and excellent crystallinity. No impurity other than $Zn_3(PO_4)_2$ is detected by XRD. It indicates that the material is pure zinc phosphate. The diffraction data are consistent with PDF file No. 33-1474. Furthermore, the average crystallite size of synthesized $Zn_3(PO_4)_2$ is 10.5 nm, as the result estimated by Scherrer's formula.

3.3. FTIR spectroscopy

The FTIR spectrum of the as-prepared material is shown in Fig. 3. There is a broad envelope between 3700 and 3000 cm^{-1} due to the O–H stretch of water. The peaks become weak and nearly disappeared at 750 °C. The intense broad peak between 900 and 1160 cm^{-1} is assigned to PO_4^{3-}. The peak at 883 cm^{-1} may be ascribed to a symmetric P–O stretching vibration of PO_4^{3-} groups and 472 cm^{-1} band results from the ν_2 phosphate mode. An observation of the spectrum which shows a shoulder at about 981 cm^{-1} in the spectrum of the as-prepared material also belongs to PO_4^{3-} groups. The stretching and bending modes of PO_4^{3-} emerge at 602 and 562 cm^{-1}.

Small C–H stretching vibration bands appear at 1438, 2859 and 2926 cm^{-1} and weak N–H peaks (608, 1629 cm^{-1}) show that there are some residual yeasts or biomacromolecules after the extraction by water and ethanol.

3.4. SEM and mechanism

Fig. 4 shows the dispersion state of the powders. Fig. 4b and c reveals that well-dispersed zinc phosphate particles (80–200 nm in size) were obtained when YCs were used. Compared with the crystallite size calculated by Scherrer's equation, it is clear that the large particle is aggregated by crystallites sized at about 10.5 nm. The particles with yeasts are smaller and more uniform than those without yeasts (Fig. 4a). Fig. 4c and d is the magnification of Fig. 4b which shows a beautiful butterflylike structure that has never been reported on zinc phosphate. The appearance of the special patterning may be ascribed to the growth of the crystal along one crystallographic axis.

From the results of XRD and SEM, it can be seen that the inducing of yeasts is an effective way to obtain zinc phosphate powders with narrow-size distribution in diameter. These benefited from the function of the yeasts in the reaction system, which served as nano-reactors and effectively controlled the particle size and size distribution, and inhibited the excess agglomeration of $Zn_3(PO_4)_2$ crystals in the process.

Surface functional groups of substrate materials play a decisive role in both nucleation and growth. Much research has been conducted to elucidate mechanisms of inorganic matter formation on a foreign surface and to determine the dispersion of the powders [23–26]. As we all know, pericellular membranes of microbial cells are made up of glycoprotein, membrane lipid and membrane protein which have many carboxyl groups [27] and hydroxyl groups [28]. Yeast cells are negatively charged [27,28] (had been tested) and could induce the formation of crystals easily.

Unlike ordinary surfactants, microbe cells operate differently from templates. The schematic diagrams of the interacting process and particulars are given in Fig. 5. The well dispersion of the powders can be understood by considering that the electronegative property was increased when yeast cells were used, and the repulsive force between the precursors would be increased at the same time. It is believed that the nonionic hydroxyl groups, carboxyl groups and other negatively charged groups on the cells may firstly bind the zinc ions through ionic–dipolar interaction when Zn^{2+} was introduced. Phosphate radicals dropped in the mixture were enveloped in zinc cations which were bonded on yeasts. Electrostatic effect and steric hindrance played a multiple role to avoid agglomeration of the product in the synthesis.

3.5. Corrosion preventive test

Corrosion preventive test methods for commercial solvent type paint were introduced in the test of the as-prepared zinc phosphate. Plates of tin coating with excluder pigment were soaked in weak solutions of NaOH, NaCl and H_2SO_4. The phenomenon was observed and the appearance of the first bubble on plates was recorded. Comparing with the traditional pigments such as commercial zinc phosphate, lead red and zinc chrome yellow, the anticorrosion performance of all prepared products is more excellent than commercial zinc phosphate, better than lead red and similar to zinc chrome yellow (Table 1). While the fine zinc phosphate was used to prepare the water based paint, improved storage stability was also obtained. As a result, the non-toxic water based paint can be produced with fine zinc phosphate without recourse to the toxic zinc chrome yellow or lead red pigments.

4. Conclusions

Zinc phosphate nano-powders with narrow-size distribution in diameter have been successfully synthesized by chemical precipitation method with yeasts as bio-templates. The as-synthesized $Zn_3(PO_4)_2$ powders with butterflylike microstructure are 10–80 nm in width and 80–200 nm in length (Fig. 4). The homogeneity in size distribution and shape of the products is probably attributed to the yeast cells.

The synthesized $Zn_3(PO_4)_2$ powders can be used as an antirust pigment and electronic luminophor. The technique can be expanded to many material systems, and it provides a general, simple, convenient, and innovative strategy for the synthesis of nanoparticles of metallic phosphates which may have special configuration that we want.

Acknowledgements

The authors thank Natural Science Foundation of China (Grant Nos. B2052140, B5050470) for the financial support; they also thank the Analytical Center of Shandong Institute of Light Industry, China, for the technological support.

References

[1] Lowenstam HA. Minerals formed by organisms. Science 1981;211(4487): 1126–30.
[2] Mann S. Biomineralization: principles and concepts in bioinorganic materials chemistry. New York: Oxford University; 2001. p. 134.

[3] Weiner S, Addadi L. Design strategies in mineralized biological materials. J Mater Chem 1997;7(5):689–702.
[4] Mann S, Ozin GA. Synthesis of inorganic materials with complex form. Nature 1996;382(6589):313–8.
[5] Ozin GA. Panoscopic materials: synthesis over 'all' length scales. Chem Commun 2000;6(6):419–32.
[6] Brown S, Sarikaya M, Johnson E. A genetic analysis of crystal growth. J Mol Biol 2000;299(3):725–35.
[7] Cha JN, Stucky GD, Morse DE, Deming TJ. Biomimetic synthesis of ordered silica structures mediated by block copolypeptides. Nature 2000;403(6767):289–92.
[8] Naik RR, Brott LL, Clarson SJ, Stone MO. Silica-precipitating peptides isolated from a combinatorial phage display library. J Nanosci Nanotechnol 2002;2(1):95–100.
[9] Douglas T. Protein engineering of a viral cage for constrained nanomaterials synthesis. Adv Mater 2002;14(6):415–8.
[10] Lee SW, Mao C, Flynn CE, Belcher AM. Ordering of quantum dots using genetically engineered viruses. Science 2002;296(5569):892–5.
[11] Cha JN. Silicatein filaments and subunits from a marine sponge direct the polymerization of silica and silicones in vitro. Proc Natl Acad Sci USA 1999;96(2):361–5.
[12] Kroger N, Deutzmann R, Sumper M. Polycationic peptides from diatom biosilica that direct silica nanosphere formation. Science 1999;286(5442): 1129–32.
[13] Brott LL. Ultrafast holographic patterning of biocatalytically formed silica. Nature 2001;413(6853):291–3.
[14] Klaus T, Joerger R, Olsson E, Granqvist CG. Silver-based crystalline nanoparticles, microbially fabricated. Proc Natl Acad Sci USA 1999;96(24):13611–4.
[15] Falini G, Fermani S, Gazzano M, Ripamonti A. Oriented crystallization of vaterite in collagenous matrices. Chem Eur J 1998;4(6):1048–52.
[16] Naoya H, Takashi K. Thin-film formation of calcium carbonate crystals: effects of functional groups of matrix polymers. Chem Mater 2001;13(2):688–93.
[17] Manoli F, Dalas E. Calcium carbonate overgrowth on elastin substrate. J Cryst Growth 1999;204(3):369–75.
[18] Manoli F, Koutsopoulos S, Dalas E. Crystallization of calcite on chitin. J Cryst Growth 1997;182(1):116–24.
[19] Rajesh RN, Sarah JS, Gunjan A, Sharon EJ, Morley OS. Biomimetic synthesis and patterning of silver nanoparticles. Nat Mater 2002;1(3):169–72.
[20] Shiwen D, Maosheng W. Studies on synthesis and mechanism of nano-$CaZn_2(PO_4)_2$ by chemical precipitation. Dyes Pigments 2008;76(1):94–6.
[21] Pawlig O, Trettin R. Synthesis and characterization of α-hopeite, $Zn_3(PO_4)_2 \cdot 4H_2O$. Mater Res Bull 1999;34(12):1959–66.
[22] Zou HT, Tang WH, Liu JP, Su YF, Yu ZF. Synthesis of zinc phosphate microcrystal bars by solid-phase chemical reaction at low temperature. Ind Min Proc 2006;35(5):19–26.
[23] Bunker BC, Rieke PC, Tarasevich BJ, Campbell AA, Graff GL. Ceramic thin-film formation on functionalized interfaces through biomimetic processing. Science 1994;264(5155):48–55.
[24] Tanahashi M, Matsuda T. Surface functional group dependence on apatite formation on self-assembled monolayers in a simulated body fluid. J Biomed Mater Res 1997;34(3):305–15.
[25] Derek EG, Amanda JK. Fossilization of soft-tissue in the laboratory. Science 1993;259(5100):1439–42.
[26] Kim HM, Miyaji FF, Kokubo T, Nakamura T. Preparation of bioactive Ti and its alloys via simple chemical surface treatment. J Biomed Mater Res 1997;32(3):409–17.
[27] Tanahashi M, Yao T, Kokubo T, Minoda M, Miyamoto T, Nakamura T, et al. Apatite coated on organic polymers by a biomimetic process: improvement in its adhesion to substrates by glow discharged treatment. J Biomed Mater Res 1995;29(3):349–58.
[28] Tachibana A, Kaneko S, Tanabe T, Yamauchi K. Rapid fabrication of keratin–hydroxyapatite hybrid sponges toward osteoblast cultivation and differentiation. Biomaterials 2005;26(3):297–303.
[29] Yu YH, Guo F, Guo HY. Studies on biomineral synthesis of SiO_2 nanostructured materials by yeast cells as templates. Acta Phys Chim Sin 2006; 22(9):1163–7.
[30] Ciftcioglu N, Bjorklund M, Kuorikoski K, Kajander EO. Nanobacteria: an infectious cause for kidney stone formation. Kidney Int 1999;56(5):1893–8.